Controlled synthesis and osmotic properties of ionosilica nanoparticles

Alysson Duarte Rodrigues, Matthieu Jacob, Véronique Gauchou, Jean-Olivier Durand, Philippe Trens, Bénédicte Prélot, Peter Hesemann

*Manuscript submitted as a **Full Paper** to **Microporous and Mesoporous Materials***

Controlled Synthesis and Osmotic Properties of Ionosilica Nanoparticles

Alysson Duarte Rodrigues,[a] Matthieu Jacob,*[b] Véronique Gauchou,[b] Jean-Olivier Durand,[a] Philippe Trens,[a] Bénédicte Prelot,[a] and Peter Hesemann*[a]

[a] Institut Charles Gerhardt, UMR 5253 Université de Montpellier - CNRS, Place Eugène Bataillon, CC1701, 34095 Montpellier Cedex 05, France

[b] Pôle D'Etude et de Recherche de Lacq (PERL), Pôle Economique 2, BP 47 - 64170 Lacq, France

*Corresponding authors : matthieu.jacob@total.com, peter.hesemann@umontpellier.fr

Abstract

Ionosilica nanoparticles are original ionic nano-objects at the interface of ionic liquids and mesoporous silica. Ionosilica nanoparticles' synthesis was achieved via sol-gel procedures exclusively from ionic trialkoxysilylated precursors without any silica source. However, the knowledge about the main synthesis parameters for a controlled synthesis of ionosilica nanoparticles remained fragmental so far. In this work, we present a systematic study for ionosilica nanoparticle formation starting from a virtually cationic silylated ammonium precursor. Due to their ionic nature, the behavior of ionic precursors considerably differs from that of conventional molecular silylated precursors. Here, we screened several reaction parameters for ionosilica nanoparticles' formation such as solvent polarity, precursor and surfactant concentrations, and temperature. Our results allow controlling the textures and architectures of ionosilica nanoparticles in terms of porosity (specific surface area) and particle size. The formed ionosilica nanoparticles were thoroughly characterized by means of nitrogen sorption, elemental analysis, electron microscopies, dynamic light scattering (DLS), and solid state NMR measurements. Liquid ^{1}H-NMR spectroscopic measurements allowed monitoring the kinetics of the hydrolysis-polycondensation reactions. It appeared that the hydrolysis is relatively fast (30-120 min) whereas the polycondensation reaction requires more time (1-2 days). Finally, we used Forward Osmosis (FO-) experiments as a valuable tool to monitor a possible evolution of the nanoparticles in aqueous media. We observed that the ionosilica nanoparticles showed decreasing osmotic properties in successive FO-regeneration cycles. We attribute these results either to the exchange of the osmotically active halide anions or to particle agglomeration. Ionosilica nanoparticles therefore show limited long-term stability in aqueous media that limit their potential as draw solute in forward osmosis.

Keywords

Ionosilica; nanoparticles; template directed synthesis; sol-gel process; forward osmosis

1. Introduction

Ionosilicas, defined as hybrid silica constituted of ionic building blocks (figure 1) [1-4], recently emerged as a new family of functional materials in the area of organic-inorganic hybrid materials. Ionosilicas are obtained via sol-gel procedures exclusively from oligosilylated ionic precursors. As a special type of organosilicas [5-10], ionosilicas combine the textural and morphological versatility of silica and the chemical flexibility of ionic liquids. On the one side, ionosilicas display an unmatched chemical polyvalence, induced by the high variability and the high number of ionic species that are homogeneously distributed within a silica hybrid matrix. Ionosilicas can therefore be considered as heterogenized and porous ionic liquids [11]. On the other side, ionosilicas can adopt various morphologies and textures, similarly to silica based materials obtained by the sol-gel process.

The chemical and physico-chemical polyvalence of ionosilicas is related to the huge number of possible cation-anion combinations. As an example, the hydrophilicity of ionosilicas principally depends on the nature of the counter-anion [12, 13]. Halide anions generate relatively hydrophilic ionosilicas whereas fluorinated anions such as *bis*-trifluoromethanesulfonimide (NTf_2^-) give rise to less hydrophilic materials [12]. However, ionosilicas are generally hydrophilic materials, similarly to ionic liquids. It is possible to tune the hydrophilicity of ionosilicas from highly to moderately hydrophilic. The high hydrophilicity of ionosilicas opens the route towards applications for example in the area of thermochemical heat storage [13]. Additionally, the high number of ionic groups that are immobilized in a reduced space gives rise to unusual confinement effects, which cannot be achieved in conventional non-ionic porous materials [14]. For example, compared to conventional silica, ionosilicas display very different affinities especially towards ionic liquids. ILs confined within conventional silica phases show bulk-like liquid behavior [15]. On the opposite, the interactions of ILs and ionosilica matrices are much stronger and result in a solid-like behavior of confined ILs, as indicated by solid-state NMR measurements [16].

.

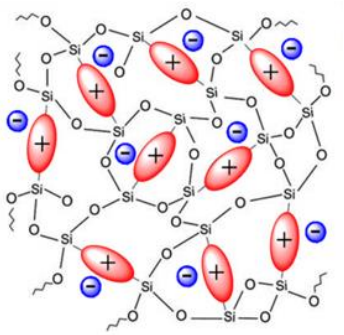

Figure 1 Chemical constitution of an ionosilica

Furthermore, ionosilicas can adopt various morphologies and textures. Ionosilicas are synthesized via hydrolysis-polycondensation reactions starting from ionic precursors. The formation of the solid occurs under kinetic control [17]. The very mild reaction conditions employed during the sol-gel process open the route toward materials displaying particular textures and morphologies [18]. In this way, the conditions of the sol-gel process allow accessing materials via bottom up-reactions staring from the molecular level. In this context, template directed syntheses are particularly versatile methods for the formation of mesoporous materials [19-22]. We reported ionosilica phases with specific surface areas in the range of several tenths of m^2/g up to more than 1000 m^2/g [23]. Materials without any structural regularity could be obtained as well as structured ionosilica phases with regular 2d-hexagonal architectures on the mesoscopic length scale. These latter materials can be considered periodic mesoporous ionosilicas and therefore belong to periodic mesoporous organosilicas (PMOs) [24]. The reaction conditions of the hydrolysis-polycondensation reactions allow controlling the architectures and morphologies of the formed ionosilicas over several orders of magnitude, from the molecular up to the macroscopic length scale [25].

Among the available morphologies that can be achieved via the sol-gel process, nanoparticles attracted particular attention. Silica nanoparticles with very narrow size distribution can be obtained by the Stöber Process and are known since the late 1960s [26]. Since then, a plethora of silica-based nanoparticles has been reported, in particular for biomedical applications [27, 28]. Examples of polysilsesquioxane based nanoparticles have also been reported [29-31].

We already reported ionosilica nanoparticles (INPs), obtained following modified Stöber-techniques. In our previous studies, we used ionosilica nanoparticles as drug carrier vehicles for anionic drugs [32, 33]. In this way, we took benefit of the unique anion exchange properties of ionosilicas [23, 34-37], combined with the possibility to efficiently control the morphology of silica hybrid materials. We observed that ionosilica nanoparticles efficiently vectorize anionic pharmaceuticals such as diclofenac, a non-steroidal anti-inflammatory drug (NSAID), or gemcitabine monophosphate, a potent anti-cancer drug. Ionosilicas display low cytotoxicity, and high hydrophilicity, resulting in good dispersibility in aqueous media. These features favor applications of INPs in *in vitro* and *in vivo* drug delivery. Ionosilica nanoparticles therefore appear as particularly polyvalent and functional nano-objects with high potential in the bio-medical field.

However, the formation of INPs is a complex process that depends on various reaction parameters such as temperature, concentration, and the presence of additives. The behavior of ionic precursors differs from that of conventional molecular silylated precursors such as tetraethyl-*ortho*-silicate (TEOS) or organosilylated compounds like 1,4-*bis*(triethoxysilyl)benzene (1,4-BTEB) or 1,2-*bis*(triethoxysilyl)ethane (BTEE), as the ionic nature of the precursor deeply impacts mechanism and kinetics of the sol-gel processes, in particular in template directed hydrolysis-polycondensation procedures. The control of texture and architecture of ionosilica nanoparticles cannot directly be transposed from classical Stöber syntheses, and the description of the main reaction parameters in INP formation remains fragmental so far. A more systematic approach for the formation of ionosilica nanoparticles is necessary in order to predict and to control the morphology of these nano-objects in terms of porosity, particle size and particle size distribution. For this reason, we report here on a systematic evaluation of several main reaction parameters in view of a controlled formation of ionosilica nanoparticles with well-defined characteristics in terms of particle size and texture.

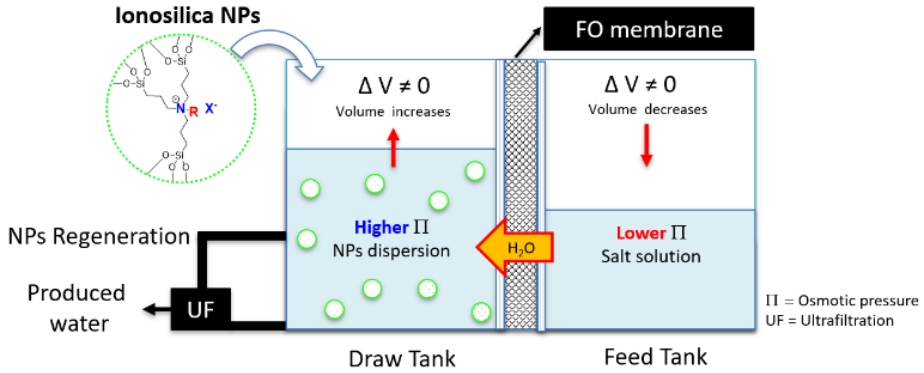

Figure 2. Closed FO-UF cycle using ionosilica nanoparticles (INPs) as draw solutes.

Finally, we report the use of ionosilica nanoparticles as draw solutes (DS) in forward osmosis (FO, figure 2). In the last few years, forward osmosis (FO) attracted increasing interest as a sustainable technique for water desalination and wastewater treatment [38, 39]. Today, FO remains as an immature process due to the lack of efficient and easily recyclable draw solutes. We were particularly inspired by the successful use of ionic liquids as DS [40-42]. Hydrophilic nanoparticles were intensively studied as draw solutes in FO in the recent past due to advantages such as easy separation and regeneration via ultrafiltration (UF), and low generated back-flux during the FO process [43-46]. The ease of separation opens the route towards the regeneration of the nanoparticles and therefore towards the design of closed osmosis-regeneration processes. However, reported data for generated osmotic properties of nanoparticles are often not reliable and sometimes even contradictory. Today, it is accepted that the osmotic pressures generated by nanoparticles are too low for a large-scale application of these systems as draw solutes in FO applications. However, macroscopic physico-chemical characteristics such as generated osmotic pressure may give insight regarding their hydrophilicity and ion mobilities of these nano-objects. Osmotic pressure therefore gives interesting information about fundamental properties of these nano-objects, their stability and their evolution in aqueous media. FO measurements with INPs therefore appears as an interesting tool to monitor the hydrophilicity of these nanoparticles and to follow their long-term stability. For this reason, we studied the use of IPNs as recyclable draw solutes in successive FO-UF regeneration cycles (scheme 1).

2. Materials and methods

2.1. Characterization methods

Liquid NMR spectroscopic data was obtained with a Bruker Advance 200 or 400 MHz spectrometers. Chemical shifts are given in parts per million (ppm) relative to tetramethylsilane. *J* values are given in hertz. Solid NMR data were obtained with a Cryomagnet (Oxford) spectrometer working at 300 MHz with around one gram of dried samples using cross polarization magical angle spinning - CP-MAS $\{^{1}H\}$-(^{13}C and ^{29}Si) and MAS ^{29}Si (one-pulse) techniques. High performance liquid chromatography (HPLC) was performed on an Alliance 2795-Waters with a mass spectrometry (MS) detection ESI-QTOF-Waters spectrometer using electro spray ionization (ESI) methods in high and low resolutions. Elemental analysis was performed using a FlashEA® 1112 (Thermo) equipment. FT-IR measurements were recorded on a Perkin Elmer FT-IR spectrometer - Spectrum Two. Dynamic light scattering (DLS) was used to estimate particles sizes using a DLS Cordouan Technologies DL 135 particle analyzer, which were later confirmed when necessary by electronic microscopy. SEM images were obtained on a Hitachi S4800 FS with a resolution of 1 nm at 15 kV. TEM images were obtained on a JEOL 2200 FS - 200 kV equipped with a CCD Gatan USC 4092x4092 px^2 camera. Surface areas of dried solids were measured on a 3FLEX Micromeritics using nitrogen as adsorbent molecule with samples outgassed during 7h at 80°C in a Smart Vac. Prep. Sample degas system equipped with a T-station 85 Edwards pump (10^3 Pa). BET (Brunauer, Emmett Teller) and BJH (Brunauer, Joyner, Halenda) methods were applied to obtain surface areas, pore sizes, pore volumes and pore size distribution curves. Osmometric measurements were realized with a freezing point osmometer (Gonotec – Osmomat 3000) with 50 microliters of samples. Solid samples were dispersed in HPLC grade water, sonicated 10 min and acidified with diluted acid solutions realized in same solvent conditions. Samples were homogenized by aid of an orbital shaker (300 rpm) during one night before osmometric measurements.

*2.2. Synthesis of tris(3-(trimethoxysilyl)propyl)amine **1***

The synthesis of tris(3-(trimethoxysilyl)propyl)amine **1** was carried out with commercial reagents without solvents in standard and oven dried Schlenk flasks under argon. It was realized by mixing (3-aminopropyl)trimethoxysilane (84.5 mL, 0.36 mol, 1 equiv.), (3-chloropropyl)trimethoxysilane (232 mL, 1.28 mol, 3.5 equiv.) and *N*-ethyl diisopropylamine (248 mL, 1.46 mol, 4 equiv.) under argon atmosphere. The light-yellow homogenous solution was stirred magnetically (600 rpm, room temperature) for five minutes prior to heating the solution at 160°C for 30h. After this time, the obtained biphasic light yellow/orange solution was cooled to room temperature (overnight) and then to 0°C in an ice bath (3h). The *N*-ethyl diisopropylammonium chloride precipitated and was eliminated by successive recrystallizations and filtrations. The resulting solution was purified by medium vacuum distillation (< 1 x10^{-3} mbar) starting from room temperature until 160°C (with increments of 20°C) until no more unreacted starting materials distillated. The final orange liquid was washed with *n*-pentane 3 times, concentrated by rotary evaporation, filtered over a 0.2-micron syringe filter (cellulose acetate) and was finally vacuum dried giving 186 mL of the title compound. Yield = 83 %. (Density: 1.0904 g/cm^3)

^{1}H NMR: ($CDCl_3$, 400MHz) δ (ppm): 3.34 (s, 27H); 2.18 (m, 6H); 1.30 (m, 6H); 0.37 (m, 6H) (ESI-figure S1); ^{13}C NMR: ($CDCl_3$, 150 MHz,) δ (ppm): 57.1, 50.5, 20.2, 6.7; HRMS [ESI+] calcd. for $C_{18}H_{46}N_1O_9Si_3$: 504.2480 [cation M+1]; found: 504.2480; IR-ATR (cm^{-1}) : 2941, 2836, 1463, 1189, 1079, 811, 779, 442. Elemental analysis: Calculated: C: 42.91; H: 9.0, N: 2.78; Found: C: 41.54; H: 8.15, N: 2.57

*2.3. Synthesis of ionosilica nanoparticles starting from **1**:*

In a typical procedure, a solution of precursor **1** (7.33 mL, 15.7 mmol) in 650 mL of 2-propanol at room temperature was directly added 350 mL of a hot aqueous solution of sodium hexadecyl sulfate (SHS) (0.65 g, 1.8 mmol) previously heated at 70°C until total dissolution of SHS (around 40 min). A homogenous yellow solution is obtained and after 15 min at 1250 rpm, nonionic

surfactant F127 (209 mg, 0.025 mmol) is added to the system. The final solution was stirred at room temperature for 2 days leading to the formation of NPs of around 13 nm. At room temperature, the NPs dispersion was cotton filtered and 2-propanol was rotary evaporated (40°C, 130 mbar). Solvent extractions with toluene or UF have been used to further remove surfactants and concentrate NPs dispersions prior FO tests.

2.4. Removal of INPs from dispersions for characterizations:

After synthesis, the dispersion containing the INPs was transferred to a separating funnel and directly extracted with isovolumic amounts of toluene. The INPs in the organic phase (toluene/2-propanol) were isolated and the aqueous phase containing most of the surfactants was eliminated. The organic layer was washed with water until removal of excess surfactants. To reduce NPs aggregation during solvent evaporation, a sucrose solution (isovolumic, 2 g/L) was added to the extracted NPs dispersion and solvents were rotary evaporated (50°C, 40 mbar). The solids were further dried under vacuum during 5h (r.t). Sucrose grains containing NPs entrapped were obtained. Prior use, NPs were in three cycles dispersed in water, sonicated (2 min) and centrifuged (10K rpm, 5 min, 20°C). A last cycle of dispersion and centrifugation was done in ethanol and after vacuum drying, NPs were characterized by the different techniques.

Solid state RMN: CP-MAS $\{^{1}H\}$-^{13}C NMR (300 MHz) - δ (ppm): 58.9, 48.2, 31.6, 21.2; 12.2, CP-MAS $\{^{1}H\}$-^{29}Si NMR (300 MHz) - δ (ppm): -49.4, -58.0, -67.5, IR-ATR (cm^{-1}): 2927, 2805, 1458, 1102, 1001, 922, 701, 452 Elemental analysis - Calculated: C: 31.32; H: 5.52, N: 3.65; S : 0.00 Found: C: 31.31; H: 5.77, N: 3.21 S: 0.78 (S from residual SHS surfactant).

2.5. FO-UF process

Experiments were conducted in a totally automatized reverse osmosis (RO) pilot adapted for FO process (scheme 2). The pilot is composed of a stainless-steel feed tank (Imeca) with a total volume capacity of 20 L containing the feed solution (aqueous NaCl, 0.1 g/L). Feed solutions were

circulated by aid of a piston pump (Lafert) working at 18-20% of its capacity and generating a circulating water flux of 60.8 (± 3.0) L/h in the feed side. Water levels in the tank, conductivities and pressures were measured automatically with values being monitored through a digital screen (Imeca) incorporated to the pilot.

Pressure variations were measured before and after feed solutions entering in the FO membrane module in the feed side. Inlet pressures showed values in the interval of 0.67 ± 0.05 bar (PT_1) and outlet pressures were in the range of 0.45 ± 0.05 bar (PT_2) during all experiments. These constant values were used to calculate the transmembrane pressure by discounting circulating pressures from the draw side (0.20 ± 0.05 bar - P_{Draw}). The transmembrane pressure during the trials was obtained (0.36 ± 0.05 bar) applying the developed formula for the calculations: $((PT_1 + PT_2)/2) - P_{Draw}$ .The stainless-steel RO membrane module (SEPA GE Osmonics) adapted for FO process is composed of a rectangular plate with a frame design (21.2 cm in length, 16.5 cm in width and 5.1 cm in height) which can be divided in two identical parts (feed and draw side). Cellulose triacetate FO membranes (Fluid Technology Solutions – FTS) having > 99.9% salt rejection, contact surface in the module = 0.0137 m^2 and with the active brighter layer turned over the feed solution were inserted in the module between two plastic grids of same sizes and thickness (1 mm) used to keep the membrane steady during FO process. Four holes in the non-contacted extremities held the membrane in the module, which was maintained closed by a pneumatic press (60 bars). The draw tank is constituted of a glass beaker of 1 L filled with at least 325 mL of aqueous NaCl draw solutions of different concentrations for pilot calibrations (ESI Figure S8 and ESI table S1) or INP dispersions in water. The beaker was equilibrated over a digital scale connected to a computer recording every minute the mass of water recovered from FO process (in grams). Draw solutions/dispersions were magnetically stirred (350 rpm) at room temperature and circulated by aid of a peristaltic pump (Masterflex L/S Cole-Parmer) working at 400% = 54.5 ± 3.0 L/h. Conductivities, pH and temperature variations were measured continuously by incorporating a portative multi analyzer (HQ40d - HACH) in the draw tank. Multiple tests with identical concentrations of aqueous NaCl in both sides (draw and feed) were

realized to find the best conditions minimizing solute backflows, pressure driven induced errors and system overheat with the best conditions described above. Water fluxes J_w (in $L.h.m^2$) were calculated using the developed formula $J_w = (\Delta V/ \Delta t).(1/S_m)$, where ΔV is the recovered mass of water in liters (L) in the interval of time Δt in hours (h). S_m is the membrane surface having a constant value of 0.0137 m^2 for all trials. Osmotic pressures of NPs dispersions (Π in atm) were estimated from a NaCl calibration curve (ESI figure S8 and ESI table S1) calculated using the developed formula $\Pi = nCRT$, where n is the number of osmotically active species (n = 2, NaCl), C is the molar concentration (mol/L), R is the universal gas constant = 0.08206 $L \cdot atm \cdot mol^{-1} \cdot K^{-1}$ and T is the temperature in Kelvin (K).

UF was used to re-concentrate NPs dispersions prior and/or after FO tests using an industrial UF pilot built for the occasion. The stainless-steel UF pilot (scheme 3) is composed of three interconnected metallic pipes (12 cm, 30 cm and 12 cm length respectively) having a 'C' shape, containing in the middle part a cylindrical ceramic UF membrane enclosed (CTI, Al_2O_3/ZrO_2 phase, 25 cm length, 1 cm external diameter, 6 mm internal diameter, 100 nm cut off). The pilot is connected by one side to a peristaltic pump (Masterflex), allowing the modular control of circulating fluxes of NPs dispersions in the system. A 500 mL beaker used as reservoir connects the other extremity of the pilot, allowing the UF of different volumes of dispersions. An exit at the middle part of the pilot allows the elimination of tangentially filtered solutions. Rigid plastic tubes (internal diameter = 6 mm) were used interconnecting both extremities of the pilot with the beaker and the pump. Tangential filtration was obtained closing a manual valve on the upper part of the pilot and monitoring circulating pressures with a digital manometer (Keller) used to register relative pressure variations (in mbar) during process. UF of NPs dispersions have been tested using circulating pressures in between 1200-2200 mbar, achieving UF fluxes in the interval of 1.37-1.60 mL/min (ESI figure S6/S7). Recorded data were treated with a computer software (Logger - Keller). Tangentially filtered solutions were recovered in a flask set over a digital scale connected to a computer recording every minute the mass of solution recovered from UF.

*2.6. ^{1}H NMR study of precursor **1** in different solvent conditions (400MHz - 24h)*

The transformation of the initially liquid precursor **1** into a solid-like material was followed by liquid ^{1}H NMR. To follow this change on state, we have mimicked an environment rich/poor in water using deuterated solvents (MeOD-(D_4) and D_2O respectively) where constant concentrations of **1** were added (3.6 μL **1** in 500 μL of solvent, C: 15.59 mM). After solvent addition using two different volume percentages of D_2O in the mixture (100% and 0.2% v/v% respectively) in two distinct tests ^{1}H NMR analysis were ran each fifteen minutes in the first hour and after this time each hour during a day completing 28 analyses. The time between preparation of initial solutions of precursor **1**, insertion of standard quartz NMR tubes into the spectrometer and the analysis settings were discounted in the plots (figure 6). NMR tubes containing solutions of precursor **1** (503.6 μL - final volume) were kept in the spectrometer in same conditions during the entire study.

3. Results and Discussion

3.1. Synthesis and Characterization of Ionosilica nanoparticles (INPs)

Ionosilica nanoparticles (INPs) were synthesized through hydrolysis-polycondensation reactions of tris-(3-(trimethoxysilyl)-propyl)-amine **1**, a neutral oligosilylated compound bearing a tertiary amine function. This compound was synthesized via a double alkylation of 3-aminopropyl-trimethoxysilane with two molecules of 3-chloropropyl trimethoxysilane [1]. The ^{1}H NMR spectrum of this compound is given in ESI figure S1.

We studied then the formation of nanoparticles exclusively from this compound. In a first time, we screened various parameters of the hydrolysis-polycondensation reaction. Due to the inherent basicity of the amine precursor **1**, the syntheses of the nanoparticles were carried out in the absence of additional basic catalysts such as ammonia or sodium hydroxide. The reactions were performed both in the presence or in the absence of porogenes, *i.e.* anionic surfactants. Anionic surfactants such as sodium hexadecyl sulfate (SHS), once added in the first steps of the hydrolysis-polycondensation reactions, may act as soft-templates inducing mesoporosity in the INPs *via* a supramolecular assembly process generating precursor-surfactant ion pairs [2-4], thus promoting the structuration process during the hydrolysis-polycondensation procedure. In the initial steps of the sol-gel reaction, the precursor **1** undergoes protonation with water, transforming the tertiary amine function into an ionic ammonium entity [R_3N^+H (X^-)]. The protonation of the amine precursor **1** and the formation of ionic ammonium species has been evidenced by osmometric and pH-metric measurements with purified NPs samples (*vide infra*, figure 7). The formed ionic ammonium precursor is able to generate ionic interactions with the anionic surfactant SHS, thus resulting in the formation of mesoporous ionosilica nanoparticles. On the other side, the nonionic PEO-PPO-PEO block copolymer (F127) allows controlling the size of the formed INPs via surface adsorption on the primary nanoparticles.

In a typical reaction, precursor **1** was dissolved in 2-propanol at room temperature and a hot aqueous solution of SHS was added. The homogenous hydro-alcoholic solution of **1** was stirred

without heating for 15 min and then the non-ionic surfactant F127 was added. The inherent basicity of the amine precursor **1** resulted in an increase of the pH of the initial hydrolysis polycondensation solutions to a value of 8.6. After two days at room temperature, the solution became turbid, indicating the formation of ionosilica nanoparticles (figure 3a).

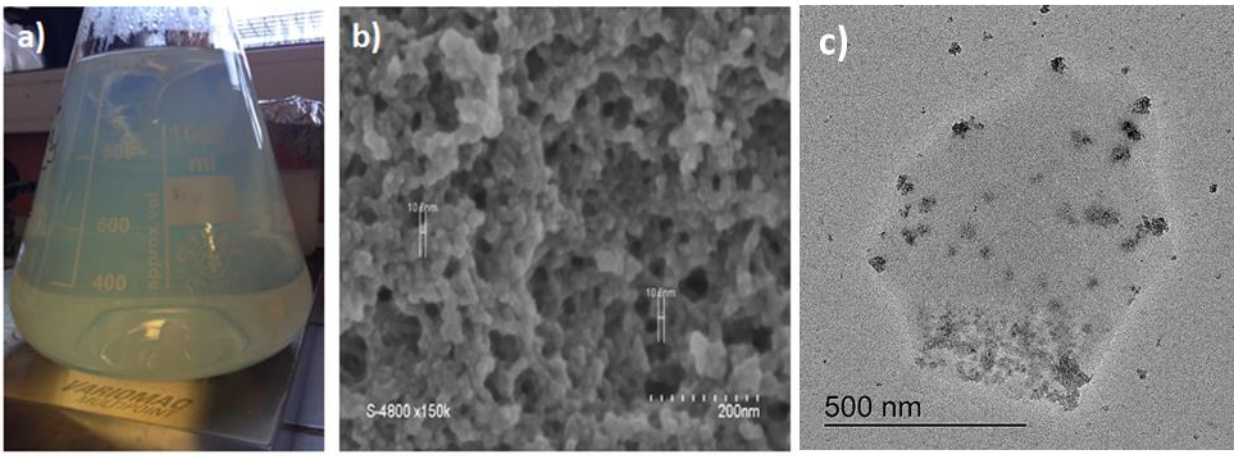

Figure 3. a) Colloidal dispersions of INPs synthesized from precursor **1** in a water/2-propanol solvent mixture b) SEM image of INPs after 48h of synthesis c) TEM image of purified and rotary evaporated INPs stabilized in a sucrose grain. INPs synthesized as given in entry 19 from table 1.

The particle size distributions of INPs were investigated *via* DLS measurements. For comparison, several samples were also investigated *via* SEM and TEM measurements. For example, DLS analysis of INPs synthesized under a specific set of reaction conditions (table 1, entry 19**)** resulted in ionosilica nanoparticles with an average size of 130 nm (ESI figure S2). On the opposite, SEM and TEM images of INPs synthesized under identical conditions (figure 3b/c, ESI figures S3a-c) indicated the formation of much smaller primary nanoparticles with average diameters of 10.5 nm and 14.2 nm, respectively. In general, DLS overestimates the diameter of the INPs if compared with the values obtained by SEM and TEM, due to surface located physisorbed F127 molecules on the INPs surfaces and/or the formation of nanoparticle agglomerates during DLS analysis. Both factors lead to an increase the hydrodynamic radius of the particles and hence an overestimation of the particle size *via* DLS.

Table 1. Screening of reaction parameters in INP synthesis from precursor **1**. The concentration of the anionic surfactant SHS was of 1.8 mmol in all trials.

N°	H_2O/2-propanol v/v%	[Prec. 1] mM/L	[F127] [mM]	T/°C	Particle size (nm)[a] – Intensity
1	94/6	8.98	0.025	r.t.	2348
2	75/25				1267
3	50/50				1187
4	45/55				314
5	40/60				289
6	35/65				192
7	30/70				0
8	25/75				0
9	7/93				0
10	35/65	1.58		50	254
11		2.74			273
12		4.18			395
13		5.63			338
14		8.98			382
15		9.96			301
16		12.85			237
17		15.74			144
18		15.74	0	r.t.	1151
19			0.025		130
20			0.047		281
21			0.22		354
22			0.39		903
23			1.62		1064
24			2.76		1143
25			3.63		1210

[a] Hydrodynamic radius (in nm) were estimated after 48h of reaction by DLS using D_{mean} intensity values.

In order to get more detailed insight in the formation and the morphology of INPs, we studied the formation of these objects as a function of various reaction parameters, *i.e.* solvent polarity (2-propanol/water volume ratio), precursor **1** concentration, concentration of neutral surfactant F127, and temperature. It clearly appeared that the reaction conditions have deep influence on the particle sizes and particle size distributions of the formed INPs (Table 1). Regarding solvent polarity, faster hydrolysis-polycondensation of precursor **1** were observed in hydro-alcoholic mixtures with higher water content, resulting in the formation of INPs with larger diameters. Particles with micrometric size were formed when water was present in more than 50% v/v in initial solutions at lower concentrations of precursor **1** (8.98 mM) and constant amounts of SHS (1.8 mM) and F127 (0.025

mM) respectively (entries 1-3). By decreasing the amount of water below 50% v/v in the systems, and while maintaining identical reaction conditions, the average size of the INPs decreased to 314 nm (45% water v/v), 289 nm (40% water v/v) and 192 nm (35% water v/v) (entries 4 - 6). With 2-propanol volume fractions > 70% v/v, we did not observe the formation of INPs even after 48h of hydrolysis-polycondensation (entries 7 - 9). It clearly results that increasing 2-propanol concentration leads to decreasing particle size (figure 4a).

Temperature was also shown to influence the morphology of INPs. The average diameter doubles from 192 nm to 382 nm when increasing the temperature of the hydrolysis-polycondensation reaction from room temperature to 50°C (entries 6 and 14).

The concentration of the ionosilica precursor **1** in the hydrolysis-polycondensation mixture has also a noticeable effect on the size of the formed particles. We studied various precursor concentrations in the range of 1.58-15.74 mmol (entries 10-17). The formed nanoparticles show diameters in the range of 150 to 400 nm. The found particle size are the lowest for the lowest and the highest precursor concentrations (entries 10/17) and go through a maximum value of ~400 nm for a concentration of 4.18 mmol of precursor **1** (entry 12, figure 3b). However, the influence of the precursor concentration on the size of the formed nanoparticles is rather low, as all formed INP are of nanometric size.

Finally, we investigated the influence of the concentration of the nonionic triblock PEO-PPO-PEO triblock-copolymer F127 on the size of the formed nanoparticles (entries 18-25, figure 4c). The presence of F127 during the hydrolysis-polycondensation reaction was shown to be necessary in view of the formation of particles with nanometric size, as microscopic particles (average diameter: 1151 nm), were formed in the absence of F127 (entry 18). The size of the formed nanoparticles goes through a minimum when low F127 concentrations were used (entries 19 - 21), and increased once more with increasing F127 concentrations (entries 22-25). These results indicate that non-ionic block-copolymers are very efficient to reduce the size of ionosilica nanoparticles, probably *via* a surface adsorption mechanism. Using higher amounts of F127, we observed another increase of the diameter

of the formed INPs, probably due to the surface adsorption of increasing amounts of the non-ionic copolymer.

In general, we could show that several parameters affect in various extent the size of the formed INPs in hydrolysis-polycondensation reactions of precursor **1**. In particular, solvent polarity, temperature and concentration of the non-ionic surfactant F127 have a clear influence on the size of the formed INPs. As our objective was to synthesize small nanoparticles, we fixed 35/65 (v/v%) water-2-propanol as solvent media, 15.74 mM of precursor **1**, 0.025 mM of F127 and 1.8 mM of SHS surfactant at room temperature (table 1, entry 19) as standard reaction conditions for our further studies. In order to get more detailed insight in their chemical and physico-chemical properties, we determined the textural and surface properties of the INPs formed under these conditions.

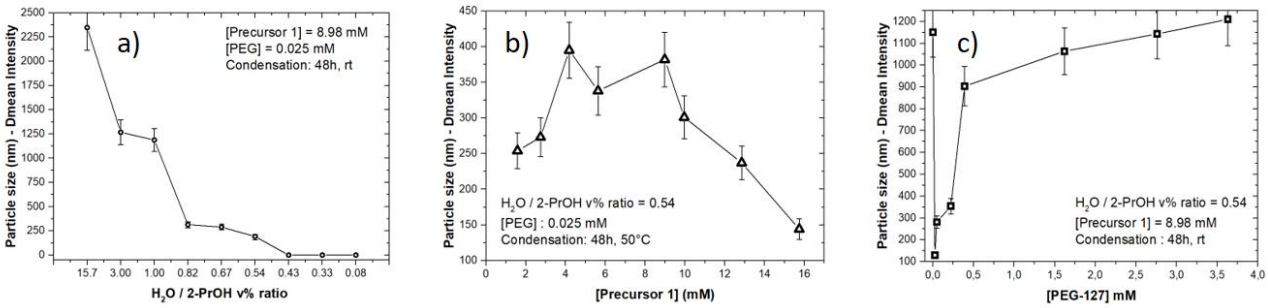

Figure 4. Evolution of the particle size of ionosilica nanoparticles as a function of solvent composition (*left*), precursor concentration (*middle*), and amount of added F127 (*right*).

The size and shape of the formed INPs was also addressed via transmission electron microscopy (TEM). The TEM images of as-synthesized INPs and purified INPs with and without sucrose stabilization are given in the ESI figure S3. Further characterization via nitrogen sorption, solid-state NMS spectroscopy and elemental analysis allowed obtaining more detailed information regarding the surface properties and the chemical constitution of the INPs.

The TEM images of as-synthesized INPs (ESI figure S3a) show nanoscopic particles of a size of around 14 nm embedded in a surfactant matrix. The surfactant corona could be eliminated by liquid extraction of the INP dispersions using toluene and water. In this way, we obtained purified INPs dispersed in 2-propanol/toluene mixture, as the nanoparticles remain in the organic phase. However,

we suppose that the excess of anionic surfactant was removed during this extraction process. However, these purified INPs form aggregated phases upon drying via solvent elimination (ESI figure S3b). This irreversible aggregation limits the application of these nano-objects, as it led to the formation of macroscopic and non-dispersible objects that finally precipitate from solution. We therefore looked for a solution that allows storing the nanoparticles over a longer period without agglomeration. We found that the irreversible aggregation process could be avoided via addition of an aqueous sucrose solution to the purified organic phase containing the INPs. Solvent evaporation led to INPs embedded in a sucrose matrix (ESI figure S3c). These phases can be stored during months without noticable nanoparticle evolution. Sucrose embedded INPs could easily be re-dispersed prior to use *via* solubilization in water or hydro-alcoholic mixtures.

Further information of the chemical constitution, composition and textural properties of the INPs were obtained via elemental analysis, solid state NMR and nitrogen sorption measurements.

The synthesis of INPs was performed on the presence of the anionic surfactant sodium hexadecylsulfate (SHS). This compound serves as a porogen for the generation of pores with controlled size. After INP formation, the anionic porogen remains inside of the pores and has to be removed for the generation of porosity. Usually, we perform solid-liquid washing processes for its removal from the ionosilica matrix, i.e. by treatment with hydrochloric acid. The amount of residual anionic surfactant (SHS) in the dried samples was addressed *via* elemental analyses, *i.e.* the determination of the nitrogen/sulfur (N/S) ratio of the materials. The as-synthesized INPs display atomic ratios N/S = 2, corresponding to two condensed amine units by one SHS surfactant molecule. This value considerably decreased after purification via liquid-liquid extraction in biphasic water/toluene-isopropanol mixtures to reach a N/S value of 9. This result confirms that the major part of the anionic surfactant is eliminated *via* the extraction process, but that 10-15% of anionic SHS remain entrapped within the INP matrix. Finally, we also synthesized INPs in the absence of SHS. As expected, elemental analysis of this material indicated the complete absence of sulphur in the sample (figure 5a).

The BET surface areas of dried samples were obtained from the nitrogen sorption isotherms (figure 5b). We observed that the removal of the porogen has clear effect on the textural properties of the material in terms of specific surface area. The results indicate a clear increase of the surface areas comparing purified samples (277 m^2/g) with the samples still containing SHS (66 m^2/g). The porosity is generated by the removal of the surfactant from the ionosilica matrix, reflecting the templating effect of the anionic surfactant in the initial synthesis steps. The material obtained in the absence of surfactant showed the lowest specific surface area in this series of materials (30 m^2/g), highlighting the importance of the porogen for the formation of porous materials (figure 5, a/b).

The removal of the porogen has also consequences on the texture of the materials in terms of pore size and pore volume. Regarding the sample after surfactant removal, an average pore size of 4.6 nm has been determined by the BJH method (desorption) confirming the mesoporosity visualized by TEM in this sample (figure 3c). Not purified INPs and INPs synthesized in the absence of surfactant show lower specific surface area and pore volumes (figure 5b). The shape of the nitrogen sorption isotherms, together with the increased pore sizes in these systems of 10.4 and 13 nm respectively, suggest interparticular porosity.

The INP samples have further been characterized by solid state NMR spectroscopy using cross polarization magical angle spinning (CP-MAS $\{^1H\}$-^{13}C) techniques. Here, we compare the three spectra obtained with the materials before and after porogen removal, and the material synthesized in the absence of SHS (figure 5c).

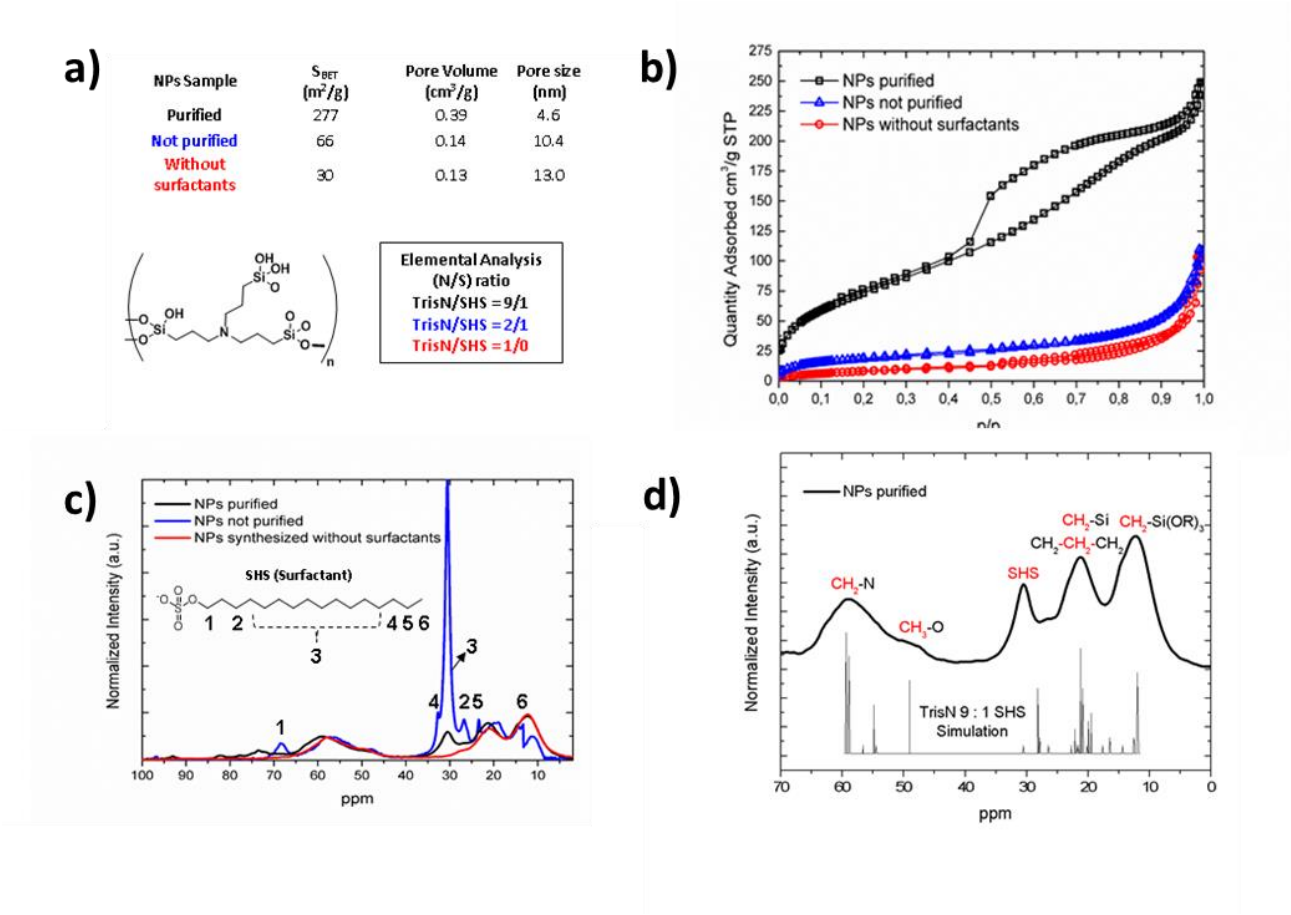

Figure 5. ***a)*** Nitrogen/sulfur atomic ratios obtained by elemental analysis with purified NPs (black), not purified NPs (blue) and NPs synthesized without surfactants (red); ***b)*** Nitrogen adsorption/desorption isotherms of purified NPs (black squares), not purified NPs (blue triangles) and NPs synthesized without surfactants (red circles); ***c)*** CP-MAS {^{1}H}-^{13}C NMR spectra of INPs: (black line) Purified NPs, (blue line) not purified NPs and (red line) NPs synthesized without surfactants in the same conditions; ***d)*** top: real CP-MAS {^{1}H}-^{13}C) NMR spectrum of purified INPs; bottom: simulated ^{13}C NMR spectrum (Chemdraw ultra 12.0 software) considering a molar ratio of 9 amine/ammonium units per 1 SHS molecule.).

First, the CP-MAS {^{1}H}-^{13}C NMR spectrum of the ionosilica material synthesized in the absence of SHS (figure 5c - red line) shows three signals at δ = 14, 21 and 58 ppm, characteristic of the propyl linkers of the amine precursor. In the spectrum of the as-synthesized sample synthesized in the presence of SHS (figure 5c - blue line), an intense peak at δ = 31 ppm indicates the presence of large quantities of anionic surfactant in this material. After the washing procedure described above, the intensity of this signal considerably decreased (figure 5c - black line), thus confirming the elimination of the major part of SHS. However, the presence of residual surfactant is confirmed by the persisting small signal at δ = 31 ppm in the spectrum of the purified sample. These results

corroborate with N/S atomic ratios from elemental analysis. ^{13}C NMR simulations with Chemdraw ultra 12.0 software considering an atomic ratio N/S = 9 led to a well-fitting model with the real CP-MAS $\{^1H\}$-^{13}C NMR spectrum of the purified sample (figure 5d). All together, the characterization of the INPs *via* CP-MAS $\{^1H\}$-^{13}C NMR spectroscopy confirms the smooth sol-gel transformation of precursor **1** and the formation of ionosilica phases from this compound.

The quantification of various silanol sites in the samples and the degree of condensation of the hybrid silica were determined using solid state ^{29}Si NMR (ESI figure S4 and table 2). The various silicon sites present in the materials were quantified using OP-(one pulse) MAS ^{29}Si NMR spectroscopy with NMR bands being firstly located with CP-MAS $\{^1H\}$-^{29}Si analysis. MAS ^{29}Si is a bulk technique allowing the overall quantification of silanol sites. Three distinct bands (**T^1**, **T^2** and **T^3**) were observed in NMR spectra (ESI figure S4) between 45 ppm < δ < 80 ppm, confirming that all silicon atoms were linked to the organic part of the compound. **T^1** band was attributed to silicon in an ($R\underline{Si}(OSi)_1(OH)_2$) environment, **$T^2$** band stands for ($R\underline{Si}(OSi)_2(OH)_1$) substructures, and **$T^3$** band refers to fully condensed ($R\underline{Si}(OSi)_3$) sites. The complete absence of signals of the Q series in the range 90-120 ppm indicates that no Si-C cleavage occurred during the hydrolysis-polycondensation procedure.

Deconvolution of the spectra was performed using DMFit software [47], allowing quantifying the amount of various condensed **T^x** species within the materials. Higher percentages of single silanol sites (Si(OH)) have been identified in not purified samples (92.2%), with contents slightly decreasing when NPs were purified (90.1%) and still reducing in materials synthesized without surfactants (87.0%). Total silanol ratio defining the number of silanols over all possible silanol sites showed the highest values in purified samples (0.65), but lower values in the case of as-synthesized material (0.51) and the one obtained in the absence of surfactant (0.59). By consequence, the condensation degree of the surfactant free sample was the lowest (0.41), whereas the two other samples show higher condensation degree (0.53 and 0.48, respectively, table 2).

Table 2. Quantification of silanol sites in samples and the degree of condensation of silica using MAS ^{29}Si NMR (one pulse) analysis - (in black) purified NPs, (in blue) not purified NPs and (in red) NPs synthesized without surfactants in identical synthesis conditions.

NP sample	Band (%)	T_2/T_3	T_1/T_3	$T_2/(T_1+T_2)$ % Single SiOH	$T_1/(T_1+T_2)$ % Geminal $Si(OH)_2$	$(2T_1+T_2)/(T_1+T_2+T_3)$ Total silanol ratio	$T_3/(T_1+T_2+T_3)$ Condensation degree
Purified	T^1 (5.90)	1.32	0.15	90.1	9.9	0.65	0.41
	T^2 (53.52)						
	T^3 (40.58)						
Not purified	T^1 (3.72)	0.83	0.07	92.2	7.8	0.51	0.53
	T^2 (43.71)						
	T^3 (52.51)						
Without SDA	T^1 (6.84)	0.96	0.14	87.0	13.0	0.59	0.48
	T^2 (45.58)						
	T^3 (47.58)						

*3.2. Kinetics of the hydrolysis-polycondensation reaction of precursor **1***

The controlled and reproducible formation of INPs is highly sensitive regarding the reaction conditions, and slight changes may result in the formation of nanoparticles with very different morphologies. As the formation of these nanoparticles occurs under kinetic control, we followed the hydrolysis-polycondensation process of precursor **1** *via* liquid ^{1}H-NMR studies in two distinct solvent compositions. The aim of this study was to evaluate the influence of the composition of the hydro-alcoholic solvent mixture on the rapidity of the hydrolysis of precursor **1** (figure 6).

^{1}H NMR experiments were run to follow the sol-gel transformation of the initially liquid precursor **1** into an hydrolyzed intermediate and finally into a solid (scheme 1). For our studies, we used constant concentrations of precursor **1** (15.59 mM) in solvent mixtures composed of D_2O and deuterated methanol (MeOD – D_4), *i.e.* 0.2% and 100% v/v of D_2O, respectively. Methanol-d_4 was used avoiding peak overlaps due to structural similarities with hydrolysable methoxysilyl (CH_3O-Si) groups of the precursor.

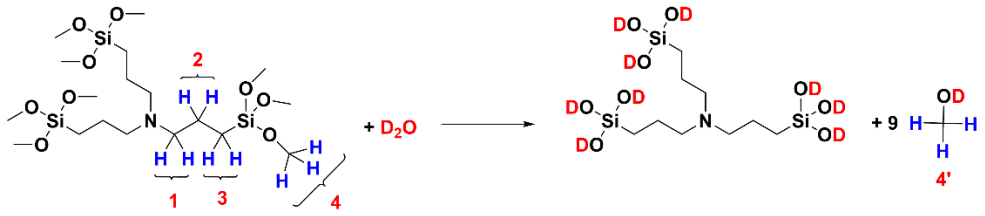

Scheme 1. Hydrolysis of precursor 1 with D_2O

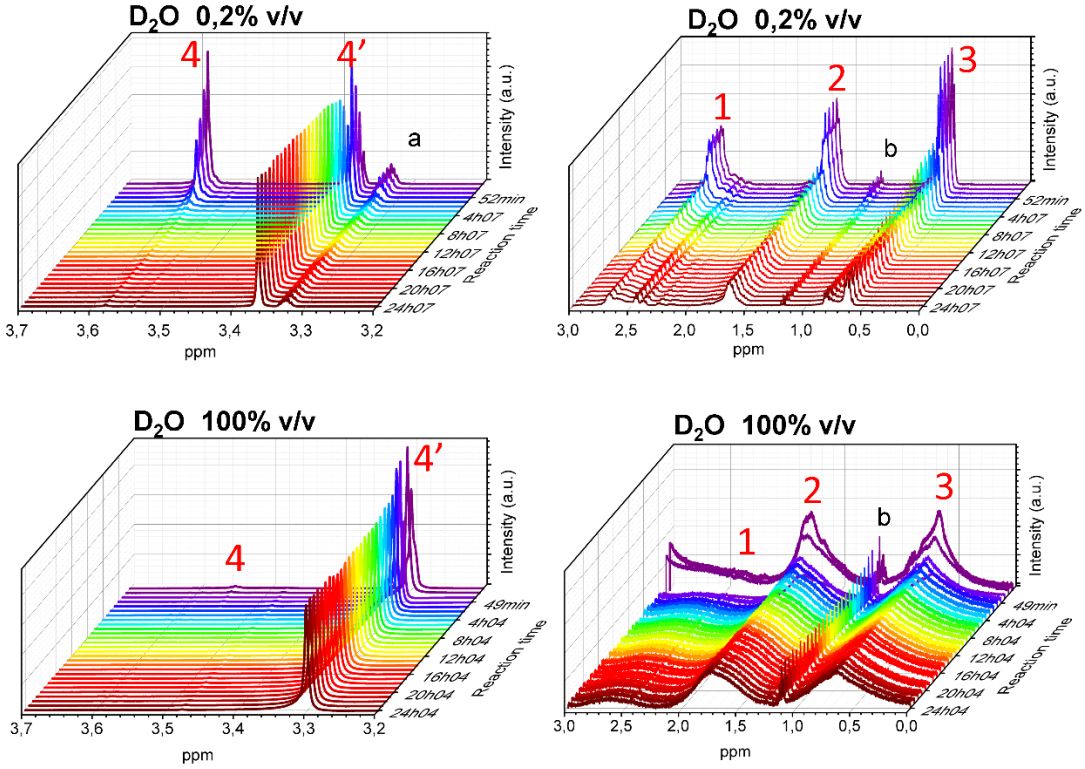

a) Impurity from MeOD: CD_2HOH
b) Impurity from D_2O : CH_3 from EtOH

Figure 6. ^{1}H NMR kinetic study of the hydrolysis of precursor **1** in different hydro-alcoholic solvent conditions and identical precursor concentrations (15.59 mM). Solvent conditions: (top) 0.2% D_2O/ 99.8% MeOD (d_4) v/v, (bottom) 100% D_2O. **1 – 3 bands =** hydrogens from the propyl chains of precursor 1 and **4' band** = hydrolyzed CH_3O- groups (**4**) from precursor **1**.

Initially, the spectrum of the molecular precursor **1** (in MeOD 99.8%) displays three multiplets at δ = 0.64, 1.63 and 2.62 ppm, corresponding to the three methylene groups in α, β and γ position relative to the silicon atom of precursor **1**. The signal at δ = 3.58 ppm can be ascribed to the three trimethoxysilyl groups of the precursor (figure 6, top).

The sol-gel transformation results in modifications of the signals related to the hydrolysable $Si(OMe)_3$ groups and the propyl chains of the precursor.

The hydrolysis of the $Si(OMe)_3$ groups occurs rapidly in both solvents. In the first trial (0.2% v/v of D_2O), the signal of the methoxy groups (**4**) progressively decreased and completely disappeared after approx. 2 h. The simultaneous formation of methanol is indicated by the appearance of a new peak at 3.36 ppm (figure 6, top (4')). The kinetics of the hydrolysis is slightly faster in pure heavy water, where complete hydrolysis is observed after 30 min. (figure 6, bottom).

These results were completed *via* the analysis of the evolution of the signals of the alkyl chains of the precursor. The relatively sharp and intense signals of all three methylene groups progressively scaled down. In D_2O, the hydrolysis process is finished after 1 h, but broad bands from the propyl chains of precursor **1** are still visible after 24 h of reaction (figure 6, bottom). This latter result reflects the fact that the more polar solvent may result in the formation of rather small ionosilica clusters that are detectable by NMR. The broadening of bands corresponds to the slow transformation of molecular precursor **1** into a solid (or nanoparticles). These INP seeds keep on growing until total consumption of the precursor in the reaction mixture.

These results indicate that the hydrolysis of the methoxysilyl groups of precursor **1** is relatively fast and is finished after approx. 1-2 h, independently form the water concentration. The polycondensation reaction is more sensitive towards the solvent composition. Slower polycondensation was observed in solution containing 0.2% v/v of D_2O. Here, more than 24h are required to complete this reaction. However, the shape of the signals suggests that oligomeric systems are formed. On the other side, the polycondensation is faster in pure heavy water. Here, the reaction is finished after 60 min. The decrease of the intensity of the signals together with their broadness suggests the formation of bigger and water insoluble objects.

3.3. Behavior of INPs dispersion acidic media: protonation or ion exchange?

Osmometric measurements combined with titrimetric evaluation of purified and re-dispersed INPs in water (figure 7) suggested that once dispersed in aqueous media, the neutral INPs obtained from precursor **1** directly undergo protonation and form tertiary ammonium-type ionosilicas (*vide supra*). This behavior was firstly indicated by the increase of pH with increasing amount of INPs in the dispersions (figure 7a), suggesting the partial formation of silica supported ammonium hydroxide species. It was confirmed *via* acidification tests of dispersions containing a variable quantity of INP with diluted nitric acid $[HNO_3]_{Final}$ = 14.6 mM. Following pH and osmolarity changes after acid addition, we observed that values did not significantly change over the whole range of INP concentrations (figure 7b and 7c – blue triangles). These results suggest that protonation of neutral amine NPs by acidic protons is not the main step involved in the formation of tertiary ammonium-type ionosilicas, but that the NPs are directly protonated by water due to the inherent basicity of the amine groups. The formation of ammonium-type INPs with different anions seems to pass through the protonation of the tertiary amine by water, followed by anion exchange under specific and selective conditions. Water plays a major role in the generation of ionic species with these hydrophilic materials. Nitrate anions seem to interact less with INPs in water resulting in constant osmolarity values (in mOsmol/Kg) over the whole range of dispersed quantities of ionosilica nanoparticles. Similar results were observed with formates whereas different results were observed with hydrochloric or hydrobromic acid (figure 7c). Acidification of INP dispersions with these latter acids gave rise to noticeable changes in pH and osmolality values: the pH increased and osmolality values decreased with increasing INP quantities (figure 7b/c). These results can be explained by classical acid/base chemistry, involving protonation of hydroxide anions by acidic protons, thus resulting in increased pH values and the modification of the osmotically active species in solution by the material. The anionic exchanges with hydrochloric or hydrobromic acid followed by the neutralization of acidic protons by hydroxide anions allowed the estimation of the average number of available ammonium cations (N^+ in mmol) per gram of material (figure 7d). This value was in average = 1.28

$mmol_{N^+}/g_{[precursor\ 1]}$, which represents 47% of the total ammonium species of the material (theoretical value = 2.71 $mmol_{N^+}/g_{[precursor\ 1]}$).

All together, these results reflect different affinities between the various anions (nitrate, formate, chloride, bromide) toward the immobilized ammonium sites. In agreement with the HSAB principle, strong interactions were observed between the hard ammonium species of the ionosilica matrix and hard anions (chloride and bromide), whereas softer anions show lower affinity towards the ionosilica matrix.

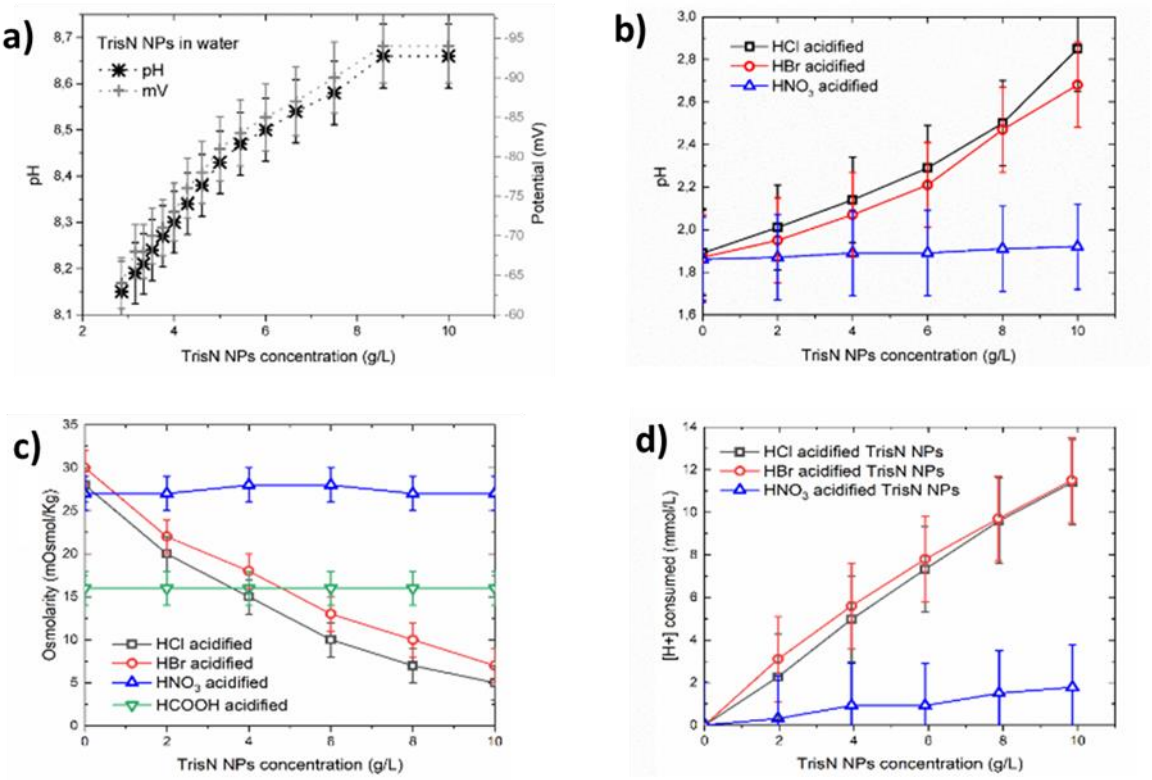

Figure 7. a) pH variation as function of INP concentration using purified INPs dispersed in ultrapure water, b) Acidification of INPs dispersions with HCl (black squares), HBr (red circles) and HNO_3 (blue triangles) at 14.6 mM respectively. c) Osmometric measurements of HCl (black squares), HBr (red circles), HNO_3 (blue triangles) and Formic acid - HCOOH (green inverse triangles) acidified dispersions of purified INPs at different NPs concentrations using identical concentrations of acid (14.6 mM). d) pHmetric quantification of consumed [H+] (in mmol/L) as function of INP concentration (in g/L) for the estimation of ammonium sites of the INPs.

3.5. FO tests with INPs bearing chloride anions (Cl^-)

We finally studied the osmotic properties of the hydrophilic INPs. More specifically, we used the INPs as draw solutes in forward osmosis (FO). In view of the elaboration of a closed osmosis/regeneration cycle, we combined the FO process with the recovery of the nanoparticles via ultrafiltration (UF).

Pilot tests combining FO-UF processes were performed with a dispersion containing 35 g/L of INPs (Cl^-). We used INPs that were synthesized in absence of anionic SDA. These simple systems were privileged in order to avoid the osmotic contribution of residual anionic surfactants, even knowing that the surface properties of the INPs are less appropriate. Pilot tests had as main objectives the evaluation of osmotic properties of the materials and the verification of the efficiency of nanoparticle regeneration via UF.

In a first time, the acidification of the INPs dispersion (initial pH 8.67) with diluted HCl (1 M) until pH values close to neutrality (pH = 6.51) ensured the formation of ionic NPs with chloride counter anions. Water production was observed during the FO process showing that ammonium chloride INPs were capable to produce osmotic pressure of 4.88 atm and draw water from feed tank at low conductivity values. For comparison, conductivities of 906 µS/cm using NaCl draw solutions would generate water fluxes in the order of 0.11 $L.h^{-1}.m^{-2}$ using identical pilot conditions (ESI figure S5). Water recovery through FO using chloride INPs led to an initial average water flux of 0.97 $L.h^{-1}.m^{-2}$ in two hours of tests what was estimated enough time to obtain a linear response from the FO pilot (ESI figure S5). Results seem to show a cooperative effect of INPs and chloride anions in the generation of higher water flux values.

After each FO cycle, the diluted dispersion of INPs was re-concentrated using UF. DI water was added restituting initial INPs concentration (35 g/L). Regeneration cycles with NPs dispersions are shown in figure 8. Six successive FO-UF cycles were performed. These successive cycles show a progressive decline of the osmotic properties, from an initial average water flux of 0.97 $L.h^{-1}.m^{-2}$ to

0.24 $L.h^{-1}.m^{-2}$ after six cycles (table 3, right column). The decrease of osmotic performance was probably related to the leaching of chloride anions from NPs along UF cycles. We suppose that chloride anions are the main osmotically active species in the system. During FO-UF cycles, chloride seems to be replaced in INPs, indicating the anionic mobility of Cl^-. This behavior is due to the observation of positive water fluxes and the increase of pH values of INP dispersion after each regeneration cycle. Conductivities were also modified along regeneration cycles, showing decreased values due to the modification of the nature of ionic species within the dispersions. (table 3)

These results suggest that the mobility of chloride anions going from the NP matrix into solution was possible but the reestablishment of the interaction with the material was probably disturbed due to a more competitive ionic environment in the draw tank. We suspect that dissolved bicarbonates coming from atmospheric carbon dioxide or others anionic species in small concentrations which were progressively introduced during DI water addition, were the probable reasons of the observed decline in osmotic properties of the materials. Another explanation is the precipitation of the draw solute *via* agglomeration of the INPs.

After six FO-UF cycles using the same INP sample, the re-acidifications of the system at more acid pH values (5.22, 4.02 and 3.05 respectively) aiming the restitution of initial water flux values were not successful (figure 8c, orange stars**)**. Only at pH = 3.05 we observed an increase of average water flux to 0.19 $L.h.m^2$, which was probably due to the influence of excess hydrochloric acid in the system.

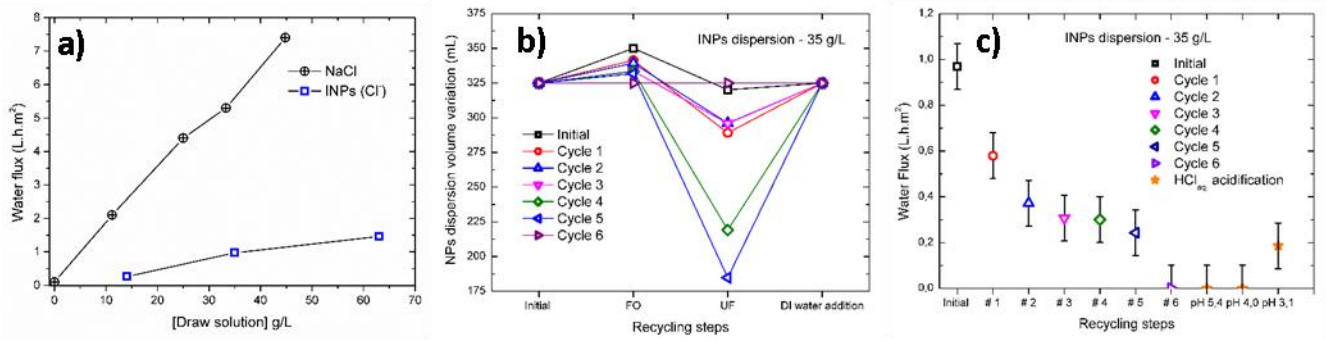

Figure 8. a) Water fluxes of NaCl solutions and INPs dispersions in water at different concentrations using same pilot configurations b) Regeneration cycles through FO-UF using a 35 g/L INPs

dispersion charge stabilized by chloride anions. c) Water fluxes (in $L.h.m^2$) as function of the regeneration cycles through FO-UF (# 1 - # 6) and by re-acidification of NPs with aqueous HCl until pH values of 5.42, 4.02 and 3.05 respectively.

Table 3. Conductivity, pH and water flux values during regeneration cycles through FO-UF with INP dispersions charge stabilized by chloride anions and after HCl re-acidification of the same INP dispersion.

INPs (Cl-) (35g/L)	**Initial Conductivity (μS/cm)**	**Initial pH**	**FO drawed water (mL)**	**UF Filtrate (mL)**	**Filtrate conductivity (μS/cm)**	**Filtrate pH**	**Water Flux $L.h.m^{-2}$**
Initial	906	6.51	25.1	29.9	34.4	6.86	**0.97**
Cycle 1	869	6.62	16.4	52.3	65.3	7.11	**0.58**
Cycle 2	889	6.63	14.3	43.2	53.1	7.32	**0.37**
Cycle 3	715	6.74	8.7	37.8	40.6	7.47	**0.31**
Cycle 4	717	6.76	8.3	114.2	25.2	7.27	**0.30**
Cycle 5	732	6.83	6.8	147	108.1	7.25	**0.24**
Cycle 6	645	6.82	0	0	-	-	**0**
HCl aq. Acidification	695	5.42	0	0	-	-	**0**
	805	4.02	0	0	-	-	**0**
	1126	3.05	2.8	0	-	-	**0.19**

4. Conclusion

We report the synthesis of mesoporous ionosilica NPs starting from an initially neutral trisilylated amine precursor. Template directed approaches with an anionic surfactant were successfully used to induce mesoporosity within the nanoparticles. Several reaction parameters were screened to obtain nanoparticles with defined surface properties. In particular, a control of NPs size distributions has been obtained by modifying the concentration of nonionic triblock-copolymer F127 to the reaction mixture. We also developed an original purification step to reduce excess surfactants and stabilize NPs after the synthesis process.

Our results evidenced the essential role of water in the protonation of the materials, transforming the initially uncharged amine containing NPs into tertiary ammonium type ionosilicas. The protonation of neutral NPs was evidenced by pH-metric and osmometric measurements suggesting that the formation of charged NPs containing different anions goes through the protonation of the materials by water (as a weak acid) followed by anionic exchanges in a selective way. Chloride and bromide presented the best anionic affinities toward the ionosilica material. The average number of available ammonium sites in purified samples was of 47 %.

Regarding osmometric measurements, chloride containing INPs generated osmotic pressure of 4.88 atm, resulting a water flux of 0.97 $L.h.m^{-2}$. The INPs were successfully recovered via UF. However, regeneration experiments in FO-UF cycles showed that the osmotic properties of the INPs progressively decreased. Regeneration of the nanoparticles via a treatment with hydrochloric acid was unsuccessful. We attribute these results to the progressive and irreversible loss of the principal osmotic vector of the nanoparticles, *i.e.* chloride anions. However, our work shows that ionosilicas can generate considerable osmotic pressure due to the presence of a high quantity of ionic species within the network.

References

[1] T.P. Nguyen, P. Hesemann, M.L.T. Thi, J.J.E. Moreau, Nanostructured polysilsesquioxanes bearing amine and ammonium groups by micelle templating using anionic surfactants, Journal of Materials Chemistry, 20 (2010) 3910-3917.
[2] S. El Hankari, B. Motos-Perez, P. Hesemann, A. Bouhaouss, J.J.E. Moreau, Pore size control and organocatalytic properties of nanostructured silica hybrid materials containing amino and ammonium groups, Journal of Materials Chemistry, 21 (2011) 6948-6955.
[3] P. Hesemann, T.P. Nguyen, S. El Hankari, Precursor Mediated Synthesis of Nanostructured Silicas: From Precursor-Surfactant Ion Pairs to Structured Materials, Materials, 7 (2014) 2978-3001.
[4] T.P. Nguyen, P. Hesemann, J.J.E. Moreau, i-Silica: Nanostructured silica hybrid materials containing imidazolium groups by hydrolysis-polycondensation of disilylated bis-N,N '-alkyl-imidazolium halides, Microporous and Mesoporous Materials, 142 (2011) 292-300.
[5] R.J.P. Corriu, J.J.E. Moreau, P. Thepot, M.W.C. Man, New mixed organic-inorganic polymers - hydrolysis and polycondensation of bis(trimethoxysilyl)organometallic precursors, Chem. Mat., 4 (1992) 1217-1224.
[6] K.J. Shea, D.A. Loy, O. Webster, Arylsesquioxane gels and related materials - new hybrids of organic and inorganic networks, J. Am. Chem. Soc., 114 (1992) 6700-6710.
[7] D.A. Loy, K.J. Shea, Bridged polysilsesquioxanes - highly porous hybrid organic-inorganic materials, Chemical Reviews, 95 (1995) 1431-1442.
[8] P. Judeinstein, C. Sanchez, Hybrid organic-inorganic materials: A land of multi-disciplinarity, Journal of Materials Chemistry, 6 (1996) 511-525.
[9] C. Sanchez, F. Ribot, Design of hydrid organic-inorganic materials synthesized via sol-gel chemistry, New Journal of Chemistry, 18 (1994) 1007-1047.
[10] P. Van der Voort, D. Esquivel, E. De Canck, F. Goethals, I. Van Driessche, F.J. Romero-Salguero, Periodic Mesoporous Organosilicas: from simple to complex bridges; a comprehensive overview of functions, morphologies and applications, Chemical Society Reviews, 42 (2013) 3913-3955.
[11] S. Zhang, K. Dokko, M. Watanabe, Porous ionic liquids: synthesis and application, Chemical Science, 6 (2015) 3684-3691.
[12] U.D. Thach, P. Trens, B. Prelot, J. Zajac, P. Hesemann, Tuning the Interfacial Properties of Mesoporous Ionosilicas: Effect of Cationic Precursor and Counter Anion, Journal of Physical Chemistry C, 120 (2016) 27412-27421.
[13] H. Wu, P. Hesemann, P. Trens, G. Silly, F. Salles, J. Zajac, Ionosilica-based anion exchangers for low-temperature thermochemical storage of energy under mild conditions of adsorbent regeneration and saturation, Chemical Engineering Journal, 398 (2020) 125634.
[14] W.Y. Zhang, Q. Zhao, J.Y. Yuan, Porous Polyelectrolytes: The Interplay of Charge and Pores for New Functionalities, Angewandte Chemie-International Edition, 57 (2018) 6754-6773.
[15] R. Goebel, P. Hesemann, J. Weber, E. Moller, A. Friedrich, S. Beuermann, A. Taubert, Surprisingly high, bulk liquid-like mobility of silica-confined ionic liquids, Physical Chemistry Chemical Physics, 11 (2009) 3653-3662.
[16] N. Abdou, A. Mehdi, N. Brun, P. Gaveau, A. Taubert, P. Hesemann, unpublished results.
[17] G. Cerveau, R.J.P. Corriu, E. Framery, Nanostructured organic-inorganic hybrid materials: Kinetic control of the texture, Chem. Mat., 13 (2001) 3373-3388.
[18] L.L. Hench, J.K. West, The sol-gel process, Chemical Reviews, 90 (1990) 33-72.
[19] J.S. Beck, J.C. Vartuli, W.J. Roth, M.E. Leonowicz, C.T. Kresge, K.D. Schmitt, C.T.W. Chu, D.H. Olson, E.W. Sheppard, S.B. McCullen, J.B. Higgins, J.L. Schlenker, A new family of mesoporous molecular-sieves prepared with liquid-crystal templates J. Am. Chem. Soc., 114 (1992) 10834-10843.
[20] C.T. Kresge, M.E. Leonowicz, W.J. Roth, J.C. Vartuli, J.S. Beck, Ordered mesoporous molecular-sieves synthesized by a liquid-crystal template mechanism, Nature, 359 (1992) 710-712.

[21] D.Y. Zhao, J.L. Feng, Q.S. Huo, N. Melosh, G.H. Fredrickson, B.F. Chmelka, G.D. Stucky, Triblock copolymer syntheses of mesoporous silica with periodic 50 to 300 angstrom pores, Science, 279 (1998) 548-552.
[22] B. Albela, L. Bonneviot, Surface molecular engineering in the confined space of templated porous silica, New Journal of Chemistry, 40 (2016) 4115-4131.
[23] U.D. Thach, B. Prelot, S. Pellet-Rostaing, Z. J., P. Hesemann, Surface Properties and Chemical Constitution as Crucial Parameters for the Sorption Properties of Ionosilicas: The Case of Chromate Adsorption, ACS Applied Nano Materials, 1 (2018) 2076-2087.
[24] F. Hoffmann, M. Cornelius, J. Morell, M. Froeba, Silica-based mesoporous organic-inorganic hybrid materials, Angewandte Chemie-International Edition, 45 (2006) 3216-3251.
[25] D. Sauvanier, W.S.J. Li, N. Ferlin, P. Lacroix-Desmazes, B. Prelot, P. Hesemann, Simple and Straightforward Synthesis of Porous Ionosilica for Efficient Chromate Adsorption, Israel Journal of Chemistry, 59 (2018) 843-851.
[26] W. Stöber, A. Fink, E. Bohn, Controlled growth of monodisperse silica spheres in micron size range, Journal of Colloid and Interface Science, 26 (1968) 62-69.
[27] Z. Li, J.C. Barnes, A. Bosoy, J.F. Stoddart, J.I. Zink, Mesoporous silica nanoparticles in biomedical applications, Chemical Society Reviews, 41 (2012) 2590-2605.
[28] F. Tang, L. Li, D. Chen, Mesoporous Silica Nanoparticles: Synthesis, Biocompatibility and Drug Delivery, Advanced Materials, 24 (2012) 1504-1534.
[29] L.C. Hu, M. Khiterer, S.J. Huang, J.C.C. Chan, J.R. Davey, K.J. Shea, Uniform, Spherical Bridged Polysilsesquioxane Nano- and Microparticles by a Nonemulsion Method, Chem. Mat., 22 (2010) 5244-5250.
[30] M. Khiterer, K.J. Shea, Spherical, monodisperse, functional bridged polysilsesquioxane nanoparticles, Nano Letters, 7 (2007) 2684-2687.
[31] J.G. Croissant, X. Cattoen, M.W.C. Man, J.O. Durand, N.M. Khashab, Syntheses and applications of periodic mesoporous organosilica nanoparticles, Nanoscale, 7 (2015) 20318-20334.
[32] R. Bouchal, M. Daurat, M. Gary-Bobo, A. Da Silva, L. Lesaffre, D. Aggad, A. Godefroy, P. Dieudonne, C. Charnay, J.O. Durand, P. Hesemann, Biocompatible Periodic Mesoporous Ionosilica Nanoparticles with Ammonium Walls: Application to Drug Delivery, ACS Applied Materials & Interfaces, 9 (2017) 32018-32025.
[33] M. Daurat, S. Rahmani, R. Bouchal, A. Akrout, J. Budimir, C. Nguyen, C. Charnay, Y. Guari, S. Richeter, L. Raehm, N. Bettache, M. Gary-Bobo, J.O. Durand, P. Hesemann, Organosilica Nanoparticles for Gemcitabine Monophosphate Delivery in Cancer Cells, ChemNanoMat, 5 (2019) 888-896.
[34] R. Bouchal, I. Miletto, U.D. Thach, B. Prelot, G. Berlier, P. Hesemann, Ionosilicas as efficient adsorbents for the separation of diclofenac and sulindac from aqueous media, New Journal of Chemistry, 40 (2016) 7620-7626.
[35] M. Petrova, M. Guigue, L. Venault, P. Moisy, P. Hesemann, Anion selectivity in ion exchange reactions with surface functionalized ionosilicas, Physical Chemistry Chemical Physics, 17 (2015) 10182-10188.
[36] U.D. Thach, P. Hesemann, G. Yang, A. Geneste, S. Le Caer, B. Prelot, Ionosilicas as efficient sorbents for anionic contaminants: Radiolytic stability and ion capacity, Journal of Colloid and Interface Science, 482 (2016) 233-239.
[37] U.D. Thach, B. Prelot, P. Hesemann, Design of ionosilicas: Tailoring ionosilicas for the efficient adsorption of p-aminosalicylate, Separation and Purification Technology, 196 (2018) 217-223.
[38] C. Klaysom, T.Y. Cath, T. Depuydt, I.F.J. Vankelecom, Forward and pressure retarded osmosis: potential solutions for global challenges in energy and water supply, Chemical Society Reviews, 42 (2013) 6959-6989.
[39] N. Akther, A. Sodiq, A. Giwa, S. Daer, H.A. Arafat, S.W. Hasan, Recent advancements in forward osmosis desalination: A review, Chemical Engineering Journal, 281 (2015) 502-522.

[40] S. Dutta, K. Nath, Prospect of ionic liquids and deep eutectic solvents as new generation draw solution in forward osmosis process, Journal of Water Process Engineering, 21 (2018) 163-176.
[41] Y. Cai, W. Shen, J. Wei, T.H. Chong, R. Wang, W.B. Krantz, A.G. Fane, X. Hu, Energy-efficient desalination by forward osmosis using responsive ionic liquid draw solutes, Environmental Science-Water Research & Technology, 1 (2015) 341-347.
[42] Y. Zhong, X. Feng, W. Chen, X. Wang, K.-W. Huang, Y. Gnanou, Z. Lai, Using UCST Ionic Liquid as a Draw Solute in Forward Osmosis to Treat High-Salinity Water, Environmental Science & Technology, 50 (2016) 1039-1045.
[43] T. Alejo, M. Arruebo, V. Carcelen, V.M. Monsalvo, V. Sebastian, Advances in draw solutes for forward osmosis: Hybrid organic-inorganic nanoparticles and conventional solutes, Chemical Engineering Journal, 309 (2017) 738-752.
[44] W.L. Ang, A.W. Mohammad, D. Johnson, N. Hilal, Forward osmosis research trends in desalination and wastewater treatment: A review of research trends over the past decade, Journal of Water Process Engineering, 31 (2019).
[45] D.J. Johnson, W.A. Suwaileh, A.W. Mohammed, N. Hilal, Osmotic's potential: An overview of draw solutes for forward osmosis, Desalination, 434 (2018) 100-120.
[46] Q. Long, Y. Jia, J. Li, J. Yang, F. Liu, J. Zheng, B. Yu, Recent Advance on Draw Solutes Development in Forward Osmosis, Processes, 6 (2018).
[47] D. Massiot, F. Fayon, M. Capron, I. King, S. Le Calve, B. Alonso, J.O. Durand, B. Bujoli, Z.H. Gan, G. Hoatson, Modelling one- and two-dimensional solid-state NMR spectra, Magn. Reson. Chem., 40 (2002) 70-76.